Spatial Profile Flattening of Ultraviolet Laser Pulses with Aspheric Refractive Optics

B.F. Murphy, P.R. Bolton, A. Brachmann, J.F. Schmerge
SLAC, Stanford, CA 94025

Abstract

The performance of an aspheric refractive beam shaping optic is evaluated with 2 picosecond pulses of 263nm wavelength from the drive laser of the SLAC Gun Test Facility radiofrequency photocathode gun. The aspheric optic is designed to convert a transverse radial Gaussian profile input into a transverse radial Fermi-Dirac profile with improved uniformity in the central region. We evaluate the correlated performance of the aspheric optic output subject to input beam position jitter to produce tolerances for input jitter based on photoinjector uniformity requirements. The position jitter tolerance of the aspheric optic is estimated to be 3% of the input beam Gaussian $1/e^2$ intensity half width to provide 90% drive laser profile uniformity.

Background

The rf gun at the Gun Test Facility is a 1.6 cell S-band photocathode structure with a space charge compensating solenoid, illuminated by 263nm wavelength pulses from a drive laser that is synchronized with the gun rf. The solenoid allows for the removal of the transverse linear space charge contribution to transverse emittance growth. Simulations indicate that emittance compensation is optimized when laser spatial intensity profile does not vary from radial uniformity by more than ten percent, meaning that the ratio of the lowest intensity to the highest intensity should be greater than ninety percent within the 1mm fixed radius.[1]

Electron bunches are extracted from the photocathode using 2 picosecond FWHM pulses of 263nm light from a frequency quadrupled Nd:glass CPA laser system sketched in Figure 1. This laser utilizes the conventional chirped pulse amplification scheme for producing energetic pulses of picosecond duration. Frequency conversion from ir to uv is achieved using a pair of type I BBO crystals. Uv pulse energies up to 500uJ can be produced with an ir input of 2.5mJ. The ultraviolet light is spatially filtered and shaped to produce the most uniform radial illumination possible at the photocathode.

Prior to this work, transverse profile shaping for this laser system has been performed by hard edge trimming of the ultraviolet beam using a two millimeter diameter iris. The iris is relay imaged to the photocathode by a pair of four meter focal length positive lenses with an effective f/# of f/200. The ultraviolet beam incident on the iris has a radial Gaussian transverse profile. With iris trimming, the variation from uniformity is determined by the Gaussian profile shape within the iris aperture. To produce a profile with an edge-to-center intensity ratio of 90% by trimming alone, only 10% of the ultraviolet light may be used (Fig. 2a.)

Alternate methods of transverse laser profile shaping include programmable microlens arrays, deformable mirrors, and aspheric refractive optics.[2] The last of these benefits from being simple to use, monolithic, and passive. An aspheric refractive optic developed by IBM[3] provides a way to increase GTF profile shaping efficiency to 68% (Fig. 2b.) The optic consists of a pair of aspheric doublet lenses, mounted in a single package. The input is a Gaussian transverse profile whose width is specific to the aspheric optic. The output is nominally a Fermi-Dirac intensity profile (Eq. 1) with β=16. We evaluate this optic ('flattener') with respect to its applicability in rf photocathode electron guns, and produce a tolerance parameter for the pulsed input beam jitter based on profile uniformity requirements.

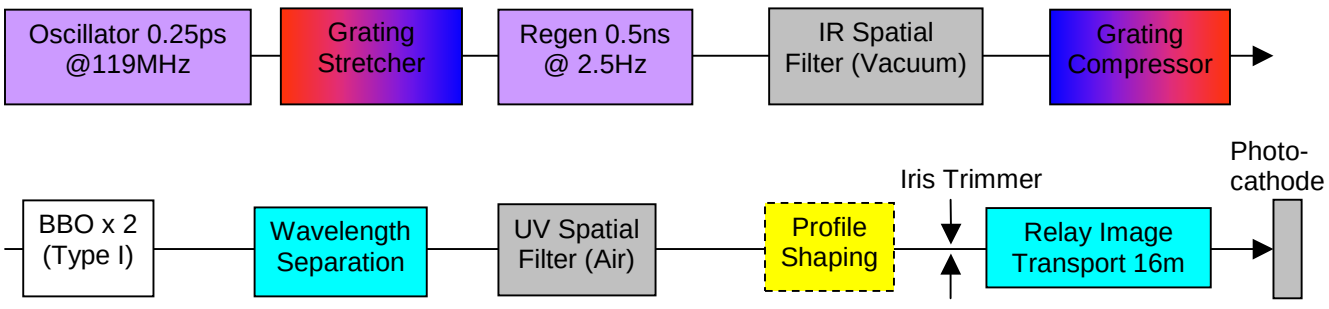

Figure 1: Layout of GTF Laser System

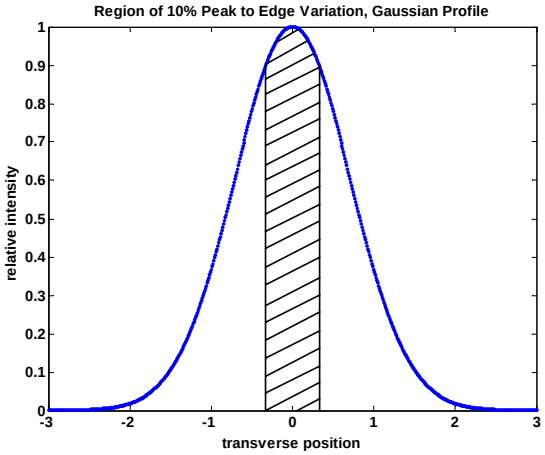

Figure 2a: Ten percent efficiency of Gaussian profiles. Transverse position in units of Gaussian width σ.

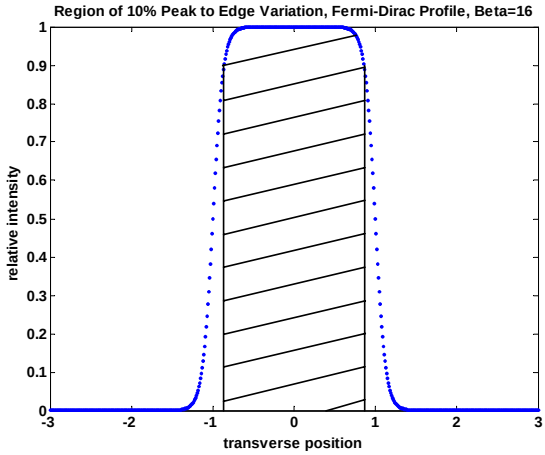

Figure 2b: Efficiency of Fermi-Dirac profile with β=16 can reach 68%. Transverse position in units of R from Eq. 1.

$$I(x) \propto \frac{1}{1+e^{\beta\left(\left|\frac{x}{R}\right|-1\right)}} \qquad (1)$$

Apparatus

In order to evaluate the feasibility of the flattener in a pulsed environment, we simultaneously measured the single pulse input and output profiles of the flattener for a series of laser pulses using the apparatus in Figure 3. Intensity profiles were recorded as 8-bit grayscale images, in bitmap format, using an externally triggered CCD camera and frame grabber. The CCD images contain both beam spots, side by side, from which positional and profile information were extracted. To accomplish this, the input beam is split into two arms by a polarizing beamsplitter cube (PBC); the relative intensity in each arm can be adjusted using a half wave plate. The reference arm (top) is imaged with a lens onto the CCD so that the profile recorded by the CCD is representative of the actual input to the flattener. In the lower arm, the flattener output is imaged directly to the same CCD, preventing propagation effects from distorting the profile. The object plane in the lower arm is about 1mm downstream of the flattener. The beam path from the uv air spatial filter to the flattener is about 2 meters, and is not relay imaged, allowing significant beam position jitter at the input to the flattener. During normal gun operation, this path is about 0.5 meters and is relay imaged. The exaggerated input beam jitter is useful in evaluating the flattener's tolerance for input misalignment.

After setting the variable expander to produce the appropriate input beam width, the flattener was aligned to produce the most uniform average output profile. Ultraviolet pulse intensity profiles were recorded and evaluated offline. This arrangement allows rapid comparison of qualitative features of the input and output, and supports quantitative correlations between input and output beam profiles.

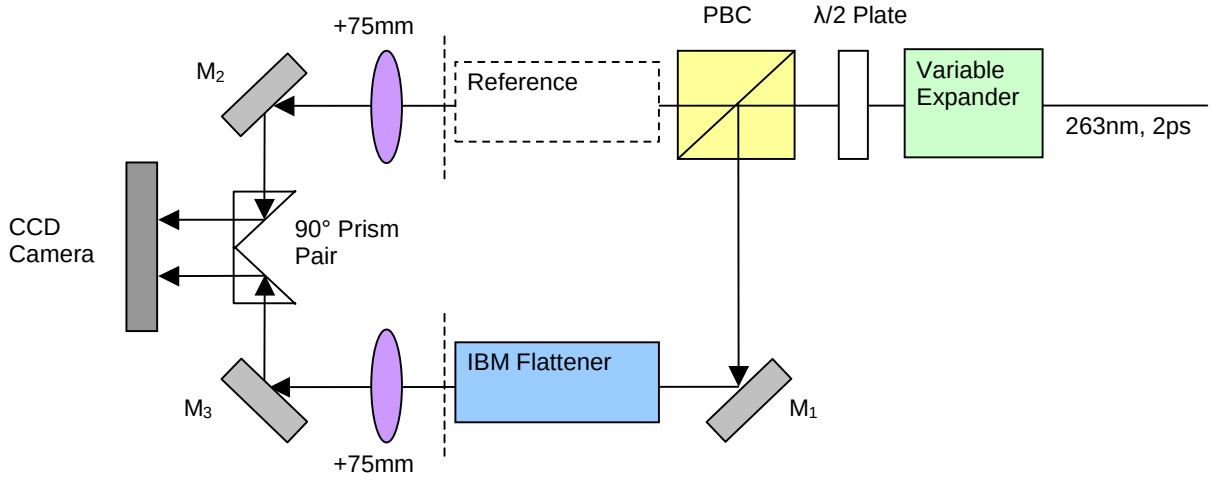

Figure 3: Experimental Apparatus.

Method

Images are read into MatLab as two dimensional 8-bit arrays for numerical analysis. Analysis proceeds through several steps, with the goal of fitting the profile to a Fermi-Dirac distribution. First, the profile centroid is calculated on both horizontal and vertical axes. Lineouts are extracted at these centroids (x lineout at the y centroid, y lineout at the x centroid) in order to evaluate the profile along both axes. The lineouts are integration normalized, and the second moment of each lineout is calculated. A series of Fermi-Dirac functions with values of β ranging from one to twenty are produced over the image pixel range, with the same centroid x_o and second moment σ^2_x as the lineout data (Eq. 2.) Coefficients c_β normalize the first integral of each function to unity. Coefficients A_β are calculated beforehand and included in the code.

$$f_\beta(x) = \frac{c_\beta}{1+e^{\beta\left(\left|x-x_0\right|/R_\beta - 1\right)}}; \quad R_\beta = \left(\frac{\int_0^{+\infty} \frac{1}{1+e^{\beta(x-1)}}\,dx}{\int_0^{+\infty} \frac{x^2}{1+e^{\beta(x-1)}}\,dx} \right)^{1/2} \quad \sigma_x = A_\beta \sigma_x \qquad (2)$$

Functions f_β are used to fit the lineout data x in a linear least squares fit, under the constraint that the fit coefficients be nonnegative (Eq. 3.)[4] The linear fit solves an eigenvalue problem in one iteration, offering better computational performance than an iterative nonlinear least squares fit in exchange for a small sacrifice of accuracy. Fit coefficients are combined to produce an average β which provides a measure of the edge rolloff and the curvature across the central 'plateau region.'

$$Fit(x) = \sum_{\beta=1}^{20} a_\beta f_\beta; \quad a_\beta \geq 0; \quad \beta_{avg} = \frac{1}{20}\sum_{\beta=1}^{20} a_\beta \beta \qquad (3)$$

Examples of high-quality Gaussian and flattened beam images donated by IBM were used to test the fitting method. Fits to these images are displayed in Figure 5. The Gaussian profile fit displays the $1/e^2$ half width of the profile along with the centroid, Fermi-Dirac beta value, and error per pixel of the fit. The flattened profile fit displays the FWHM (Eq. 4,) the centroid value, the average beta value, and Fermi-Dirac fit error per pixel. In addition it fits a line in red to the central region of the profile to calculate the slope across the plateau region. The plateau region is defined as 1.4 times the second moment of the lineout distribution, and typically excludes the rolloff region for fits with β greater than eight.

$$FWHM_x = \left(\sum_{\beta=1}^{20} a_\beta A_\beta \right) \sigma_x \qquad (4)$$

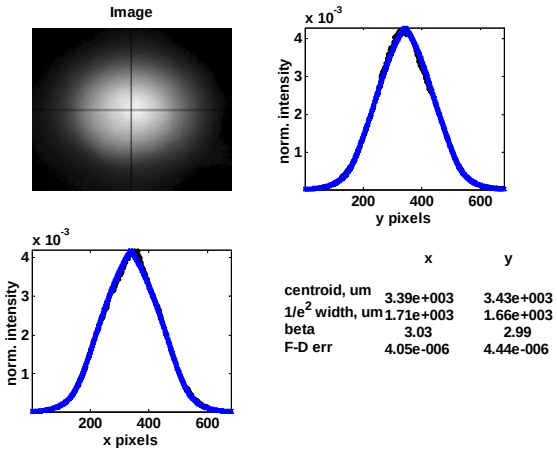

Figure 5a: IBM Flattener input profile with lineout fit. Data (black) are fit with Fermi-Dirac functions (blue.)

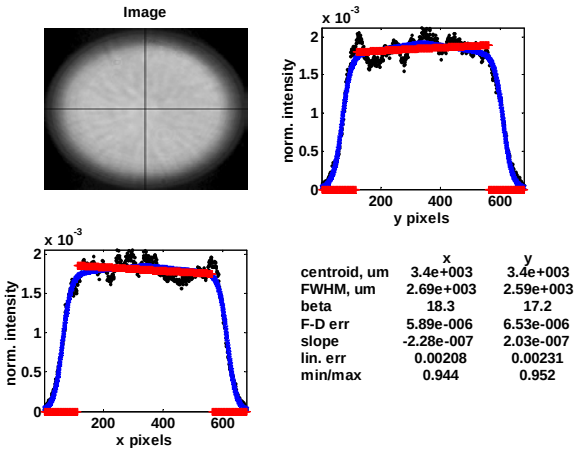

Figure 5b: IBM Flattener output profile with lineout fit. Data (black) are fit with Fermi-Dirac functions (blue) and line segments (central red.)

Experimental Data

A sample CCD image from the GTF laser is shown in Figure 6. The bright random pattern in the upper center of the image is due to prior CCD damage, and is ignored in the image processing. Background CCD intensity outside the damaged region was low, and therefore could be ignored. The smaller beam spot (Fig. 5, left) includes approximately 100 pixels along each axis, substantially fewer than in the test images, but enough for fitting. Sample fits from the experimental data are shown in Figure 7.

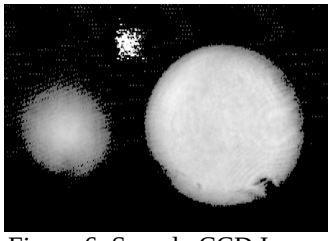

Figure 6: Sample CCD Image

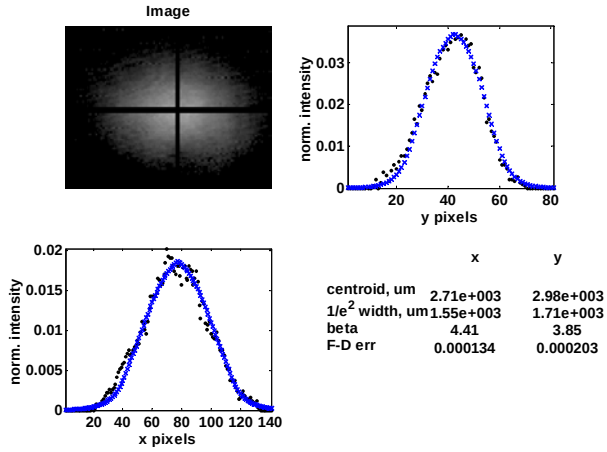

	x	y
centroid, um	2.71e+003	2.98e+003
$1/e^2$ width, um	1.55e+003	1.71e+003
beta	4.41	3.85
F-D err	0.000134	0.000203

Figure 7a: Example of GTF Flattener input profile with lineout fit. Data (black) are fit with Fermi-Dirac functions (blue.)

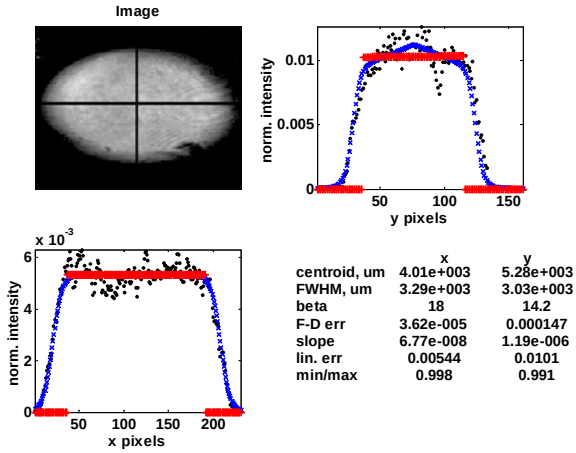

	x	y
centroid, um	4.01e+003	5.28e+003
FWHM, um	3.29e+003	3.03e+003
beta	18	14.2
F-D err	3.62e-005	0.000147
slope	6.77e-008	1.19e-006
lin. err	0.00544	0.0101
min/max	0.998	0.991

Figure 7b: Example of GTF Flattener output profile with lineout fit. Data (black) are fit with Fermi-Dirac functions (blue) and line segments (central red.)

A series of twenty shots are analyzed to produce correlation plots of input versus output parameters. Plotting the output centroid position versus the input centroid position along the x axis indicates that the effective magnification of the flattener is 1.76 (Figure 8.) The negative slope of the line in Figure 8 indicates an inverting imaging system. The magnification calculated by comparing centroid positions is largely a result of a linear slope on the plateau region of the flattener output. The edges of the output profile move very little as a function of input centroid position; the plateau slope is the dominant effect of input centroid jitter. Plotting the output plateau slope versus input position highlights this effect (Figure 9.)

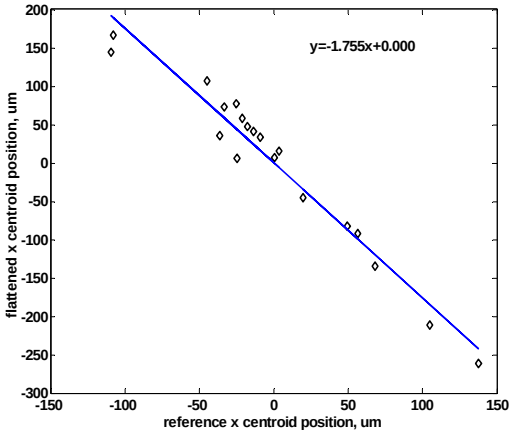

Figure 8: Output Centroid Position vs. Input Centroid Position.

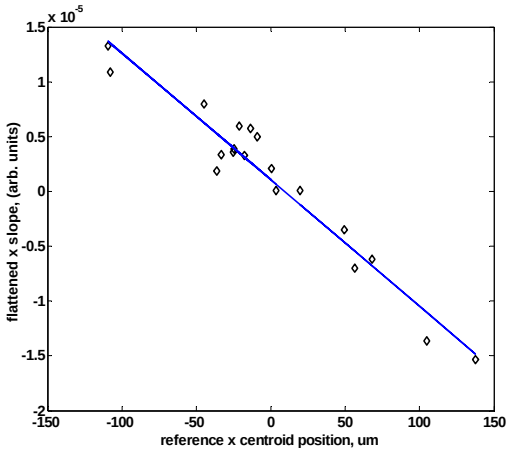

Figure 9: Output Linear Slope vs. Input Centroid Position.

A slope of zero corresponds to the case of optimum beam alignment. As the input beam position jitters about this optimum position, a variable nonzero slope can be seen on the plateau region of the flattened output on a shot-to-shot basis. This 'rocking' slope is the largest deviation from radial uniformity observed in our experiment, and can be used to estimate the flattener's tolerance for input position jitter. This was the motivation for including a linear fit in the profile analysis. Dividing the minimum fit value by the maximum fit value in the linear fit region yields a uniformity ratio which is not sensitive to measurement noise. The data in Figure 9 can thus be presented in terms of the required profile uniformity. A plot of the min./max. ratio versus input position, shown in Figure 10, places approximate limits on the jitter at ±50μm or 3% of the input beam $1/e^2$ half width in order to satisfy the 90% uniformity constraint.

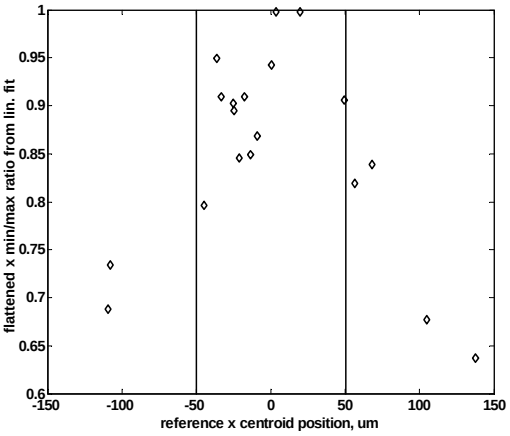

Figure 10: Input Jitter Tolerance of IBM Flattener

Conclusions

The position jitter tolerance of the IBM flattener is estimated to be 3% of the input beam $1/e^2$ half width in order to fulfill the specified 90% drive laser profile uniformity. Position jitter in the trimming iris plane of the GTF drive laser has been measured to be 2% of the ultraviolet beam profile half width, so the flattener is compatible with the GTF laser. The transmission of the flattener was measured to be 94%, with an output intensity FWHM of 3mm. If this flattener were followed by a 2mm iris as in Figure 1, the transmission would be 41%. This compares favorably with the 10% transmission of iris trimming of Gaussian profiles. A flattener designed for a 2.5mm output FWHM with β=16 would increase this transmission to 59% without adding significant curvature at the profile edge. Because edge curvature present in the optimally aligned case will add to the linear slope from shot-to-shot positional misalignment, full realization of the improved iris transmission (up to 68% with an optic designed for 2.32mm output FWHM) is only possible when shot-to-shot misalignments are negligible. In order to meet the flattener's input criteria (smooth Gaussian of specified width) it is necessary to spatially filter out ~5% of the uv energy generated in the second BBO crystal. This leads to overall profile shaping efficiencies from the uv generating crystals to the trimming iris as listed in Table 1.

Flattener Output FWHM, mm	Flattener plus 2mm Iris Transmission	Overall Profile Shaping Efficiency
3.00	0.41	0.39
2.50	0.59	0.56
2.32	0.68	0.64

Table 1: Profile Shaping Efficiency versus Flattener Output FWHM.

The MatLab program developed to fit beam profiles with Fermi-Dirac functions may be useful as a drive laser diagnostic. The beam profile display updates at about 4Hz when opening saved image files, and could be coupled to a frame grabber as a shot-to-shot beam display. Integrated with picomotor mirror controllers in a feedback system, this program could suppress slow drift (minutes to hours) degradation of drive laser profile quality in a dedicated photoinjector. It also allows for shot to shot correlations between laser and electron beam properties.

References

[1] Private communication with C. Limborg
[2] See proceedings of *Laser Issues in Rf Electron Photoinjectors*, SLAC, Stanford CA Oct. 2002
[3] J.A. Hoffnagle and C.M. Jefferson, Applied Optics **39** 30, Oct. 2000
[4] 'lsqnonneg.m' The MathWorks Inc.